Detection and volume estimation of semiconductor quantum dots from atomic force microscope images

Sangwook Oh, Chankyeong Hyon, Sanghoon Sull,[a] and Sungwoo Hwang[b]
Department of Electronic and Computer Engineering, Korea University, Anam, Sungbuk, Seoul 136-075, Korea

Yongju Park
Semiconductor Materials Laboratory, Nanodevice Research Center, Korea Institute of Science and Technology, P.O. Box 131, Cheongryang, Seoul 130-650, Korea

(Received 9 April 2003; accepted 17 August 2003)

An automated quantum dot detection and volume estimation method of atomic force microscope images are proposed and implemented. Quantum dot detection is based on the image-segmentation method widely used in image processing. We used a modified local watershed algorithm, which produces stable and effective segmentation results in order to detect the peak position of the quantum dot of the atomic force microscopy image. An effective volume estimation of the quantum dot is performed by intelligently determining the boundary of the quantum dot at each height step and by simply adding small volume fractions lying inside of the quantum dot boundary. Our volume estimation results are quantitatively analyzed by comparison with the quantum dot volume obtained by assuming conical and pyramidal shapes. The detection results of our method are quantitatively compared with the results of two other methods for general grain detection, and with a transmission electron micrograph of the quantum dot. Finally, information such as the number of quantum dots, the density, the size and the height distribution are also provided as a result of implementing our method. This method can be applied to detect and estimate volume of a similar shape with a different size. © *2003 American Institute of Physics.* [DOI: 10.1063/1.1618015]

I. INTRODUCTION

The atomic force microscopy (AFM) is the most widely used instrument among recently introduced scanning probe microscopy (SPM) techniques.[1] The widespread use of the AFM is attributed to the accurate three-dimensional reconstruction of the sample topography with atomic resolution for a relatively low cost and within a short time. Another important reason for widespread use is that there is almost no restriction on the sample to be imaged.[2]

Although the SPM can image the sample surface with atomic resolution, different types of distortion are introduced during the measurement. Generally observed sources of the distortion are for example, the tilt of sample, the nonlinear response of the piezo scanner, the thermal drift, the convolution effect of the tips, and the addition of spatial frequency noise components. A solution to these problems will be improvement of the hardware. Advances in the instrumentation hardware contribute to the high-quality AFM data acquisition. Significant improvement in the measurement accuracy and scan speed is achieved, for example, by the advanced control system that employs a state-of-the-art digital signal processor, a fast digital to analog converter and an analog to digital converter.[3] On the other hand, AFM equipment is employing piezo scanners with a different concept; the z scanner is separated from the $x-y$ scanner. More importantly, early pioneering groups engaged in the development of the AFM resolved those problems by introducing various image processing techniques, such as filtering or customized correction methods for each problem, providing ways to analyze and interpret more accurately the geometry of the surface.[4–8] However, so far, most of the data processing techniques have been used to improve the quality of raw data and they have rarely been applied to any type of more advanced data analysis.

Many scientists find a use for the AFM in different areas. Semiconductors, biotechnology, life sciences, materials, and surface characterizations are typical applications.[9–11] In most of the cases, morphology study is the main purpose of the AFM since it provides almost real three dimensional topographic information. Furthermore, the AFM data contain important information for structural analysis of the surface. For example, the AFM is considered a powerful tool for morphology analysis of nanoscale structures such as quantum dots (QDs).[12] The size, height, and density of QDs are critical since they determine the characteristics of devices fabricated with these QDs. Therefore, the determination of those parameters should always be carried on after the growth of QDs.[13] Even though algorithms exist for general grain detection, so far there is no specific tool for automatic QD detection and we must rely on manual detection of the position and size of QDs.[12] Moreover, the manual size determination process strongly depends on the user's decision, and there exists a possibility for errors in the size determination process. Therefore, we need a more reliable method independent of the user's decision. Although the well-trained user can

[a]Electronic mail: sull@mpeg.korea.ac.kr
[b]Electronic mail: swhwang@korea.ac.kr

easily identify the position of QDs by the difference in the image contrast, there is no specific algorithm to point out the position of QDs. Volume calculation of QD is also important since we can estimate the amount of source material consumed in the formation of QDs.[12]

In this article, properties of the AFM data containing QDs are analyzed, and then a QD position detection and area determination algorithm based on the modified watershed method is proposed. Once the areas of QDs have been determined, we use the result to calculate the volume of QDs. Finally, the proposed QD detection, area determination, and volume calculation are applied to various images containing QDs with different density and results are quantitatively compared to ascertain the effectiveness of the algorithm.

II. QD DETECTION AND VOLUME ESTIMATION SCHEME

A. General aspects of the AFM image containing QDs

The AFM image is a two-dimensional representation of the three-dimensional topography of sample surfaces with respect to a scan coordinate system (SCS). The probe makes a soft contact with the sample and is raster scanned parallel to the $x-y$ plane of the SCS while maintaining the contact force between the sample and the probe to a set point by relying on an electronic feedback system. The variation in the z direction, which corresponds to the height data, is monitored and stored at each particular sampling point (x,y).[14] Therefore the AFM image is a two-dimensional array of these height data or pixels where the value of each pixel corresponds to the contrast of the gray scale image. If the surface of interest has a perfectly terminated crystalline structure, such as Si or GaAs, the AFM image will be very flat with almost no variation in height. The addition of QDs to the flat surface will introduce relatively regular structures with a lateral dimension of several tens of nanometers, and local height variation will be observed in the AFM images containing QDs. The variation of the height is manifested by the contrast change, whereas the region without QDs remains a flat area where the height variation is minimum. Therefore, whenever a QD is present in an AFM image, it is easily distinguished or ''segmented'' by the difference in the contrast around the dot.

Figure 1(a) shows a typical AFM image of GaAs surface containing QDs. There are 169 randomly distributed QDs easily discernible by the naked eye and almost circular bases (bottom part of the QD) are noticed. As the height level increases, the top of small QDs is met first and then larger QDs. Bright spots correspond to the upper part of the QDs whose diameter ranges from 20 to 62 nm, meanwhile the height (base to top) of the QDs ranges from 4 to 14 nm. Therefore, the automatic position detection reduces to finding out points that have local maxima in height, which is the key aspect of the detection. The histogram of the relative height distribution is shown in Fig. 1(b). The height of the surface area is distributed in the range from 0 to 5 nm, which corresponds to black to dark gray level in the AFM image, respectively. Almost 85% of the data are in this region. The rest corresponding to QDs area have a height ranging from 4 to 14 nm, which corresponds to light gray to white level, respectively. We should pay attention to the height range between 4 and 5 nm where the height data are the combination of relatively high surface area and the base area (bottom part) of QDs. Therefore, QD detection reduces to an effective separation of QDs from the base area, which is the essence of this article.

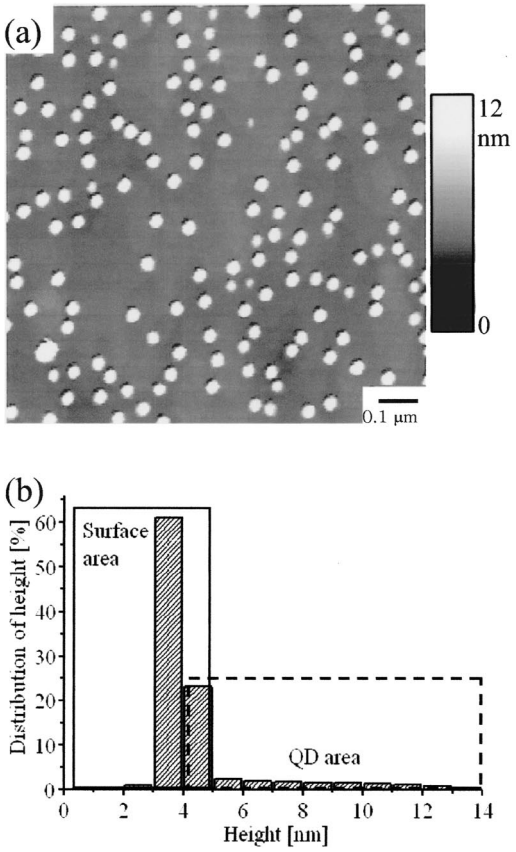

FIG. 1. (a) AFM image of InAs QDs on GaAs (100) substrate and (b) corresponding distribution of the height data.

B. Image segmentation method and QDs detection

In the image processing area, objects in the image are separated or segmented from the background by the segmentation algorithm, which can separate mutually exclusive homogeneous regions of interest. Image segmentation algorithms generally are based on one of two basic properties of intensity values: discontinuity and similarity. In the first category, the approach is to partition an image based on abrupt changes in intensity, such as edges in an image. The principle approaches in the second category are based on partitioning an image into regions that are similar according to a set of predefined criteria. Thresholding, region growing, and region splitting and merging are examples of methods in this category.[15]

In many image segmentation algorithms, we describe an approach based on the morphological watersheds, which produce more stable segmentation results than other algorithms. The watershed algorithm, which is an important morphological tool for image segmentation, has been widely used in recent years.[16–18] The watershed technique is a region-

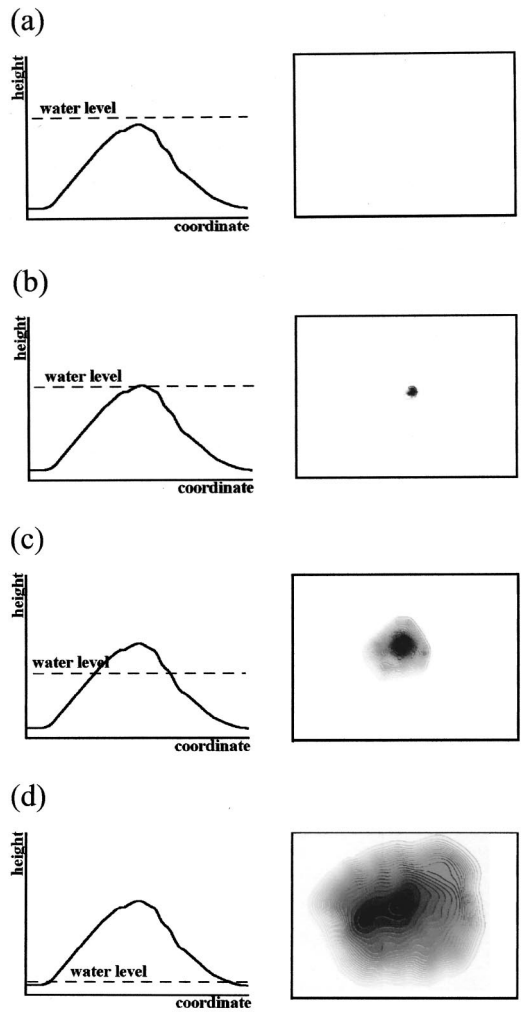

FIG. 2. (a) Concept image for islands submerged into water in the beginning, (b) image for revealed peak of island, (c) image for revealed regions of island, and (d) image for almost totally or totally revealed region of island.

growing algorithm that analyzes an image as a topographic surface.[15,19,20] It detects minima of the gradient of the pixel value and grows these minima according to the gradient values. It can be regarded as a water flooding process. The basic idea is simple: suppose that a hole is punched in each local minimum and that the entire topography is flooded from below by letting water rise through the holes at a uniform rate. When the rising water in distinct catchment basins is about to merge, a dam is built to prevent the merging. The flooding will eventually reach a stage where only the tops of the dams are visible above the water line. These dam boundaries correspond to the watershed line. Therefore, these watershed lines are the boundaries extracted by a watershed segmentation algorithm. Eventually, if there are some islands, peaks of the islands are only revealed as points.

We propose the modified watershed algorithm that uses an inverse flooding process for QD detection, which is shown in Fig. 2. Suppose that there are islands and all islands are submerged into water in the beginning. As the floodwater gradually subsides, the peaks of the islands are revealed first [Fig. 2(b)] and more regions of the island are revealed gradually [Fig. 2(c)]. Finally, the water disappears and all regions of island are revealed [Fig. 2(d)]. QDs in the AFM image can be considered as islands in this concept.

The watershed algorithm often leads to extreme oversegmentation.[19] For example, protrusions in flat regions or noises are easily detected as QD peaks. There are two approaches to reduce this problem. The first approach involves merging adjacent regions according to some criteria after the use of the watershed algorithm.[16–18] The second approach extends the watershed algorithm to deal with markers to reduce oversegmentation.[20] Markers are a set of components marking object regions of an image; i.e., each marker indicates the presence of an object. A marker represents the interior of an object. We use the second method in the proposed algorithm to prevent oversegmentation since the second method can be simply implemented in the proposed algorithm. We can impose the detected local maxima in the image and their parameters as markers.

C. QD detection with modified watershed algorithm using local maxima

In the previous section, we proposed and introduced the basic concept of the modified watershed algorithm to detect QDs in the image using local maxima. The modified watershed algorithm can be simply implemented and the performance in detecting QDs in AFM image is very effective.

We define an AFM image as I and the normalized pixel value as $g(x,y)$. The MAX and MIN are used to denote the maximum and minimum pixel values of image I, and the subsiding process goes down from $n=\mathrm{MAX}+1$ to $n=\mathrm{MIN}$. The topography will come out with water level decrements, from $n=\mathrm{MAX}+1$ to $n=\mathrm{MIN}$.

Let $M_1, M_2,\ldots,M_{C\,\max}$ be sets denoting the coordinates of points in the regional maxima of an image I and C max be the total number of regional maxima in the image. Then let $R_n(M_i)$ be a set denoting the coordinates of the points in the region associated with regional maximum M_i at stage n. And at any step n of the subsiding process, the algorithm searches pixels whose value is equal to the water level. Let $T[n]$ represents the set of coordinates (x,y) for which $g(x,y)=n$. That is,

$$T[n]=\{(x,y)|g(x,y)=n\}. \tag{1}$$

Geometrically, $T[n]$ is the set of coordinates of points in I lying on the nth plane. If we let $T_{M_i}[n]$ denote the set of coordinates of points associated with regional maximum M_i that are subsided at stage n:

$$T_{M_i}[n]=\{(x,y)|g(x,y)=n$$

and

$$\mathrm{Neighbor}_n(x,y)=R_{n+1}(M_i)\}. \tag{2}$$

Herein, $\mathrm{Neighbor}_n(s,t)$ indicates what is the neighbor of (x,y) using 3×3 pixel window at stage n. We define $\mathrm{Neighbor}_n(x,y)$ as

$$\text{Neighbor}_n(x,y)=\begin{cases} R_{n+1}(M_i), & \text{if } 3\times 3 \text{ window contains one or more pixels of } R_{n+1}(M_i) \\ \text{NEW} & \text{if } 3\times 3 \text{ window contains no regional pixel} \\ 0 & \text{if } 3\times 3 \text{ window contains pixels of } R_{n+1}(M_i) \text{ and } R_{n+1}(M_j), i\neq j \quad (1\leqslant i,j\leqslant C) \end{cases} . \tag{3}$$

Every M has a different height value. For usual watershed algorithms, preprocessing for finding all of M in the image is needed. But this preprocessing is exhaustive and duplicative. We use the $\text{Neighbor}_n(x,y)$ to find the neighbor and detect a regional maximum dynamically. From the definition of $\text{Neighbor}_n(x,y)$, each pixel of $\text{Neighbor}_n(x,y)=R_{n+1}(M_i)$ in $T[n]$ is assigned to $R_n(M_i)$ and when $\text{Neighbor}_n(x,y)$ is NEW, the new regional maximum $R_n(M_{c+1})$ is dynamically created at stage n and the pixel of $\text{Neighbor}_n(x,y)=\text{NEW}$ is assigned to $R_n(M_{c+1})$. (Here, NEW is simply a flag). C is increased to $C+1$. If $\text{Neighbor}_n(x,y)$ is zero, this means that (x,y) is a boundary pixel among some $R_n(M_i)$. In this case, (x,y) is not assigned to any $R_n(M_i)$. $R_n(M_i)$ can be obtained from

$$R_n(M_i)=\bigcup_{k=\text{MAX}+1}^{n} T_{M_i}[k]. \tag{4}$$

It is easy to see that the elements in $R_n(M_i)$ are not replaced during execution of the algorithm, and that the number of elements in this set either increases or remains the same as n decreases. Thus, Eq. (4) can be replaced as

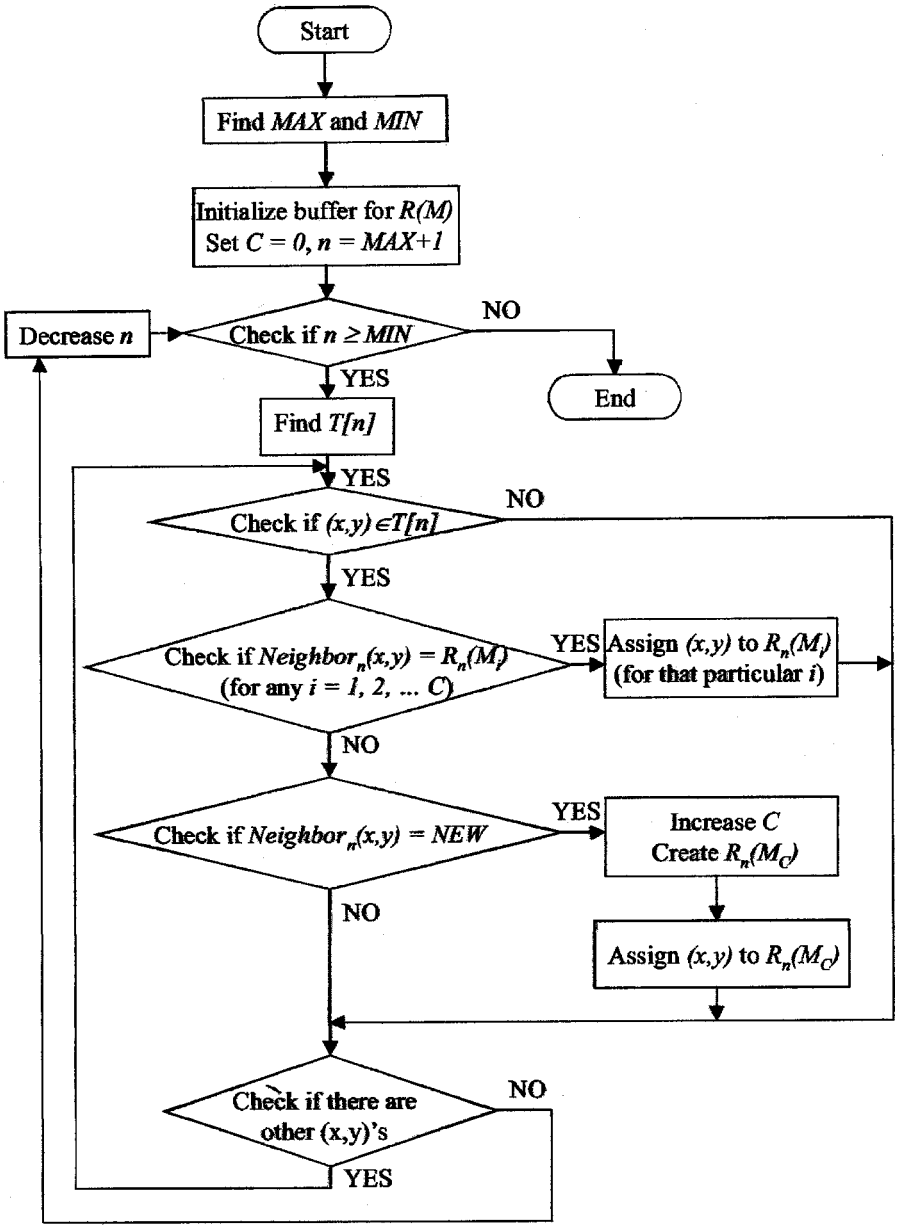

FIG. 3. Flowchart of the proposed QD detection algorithm.

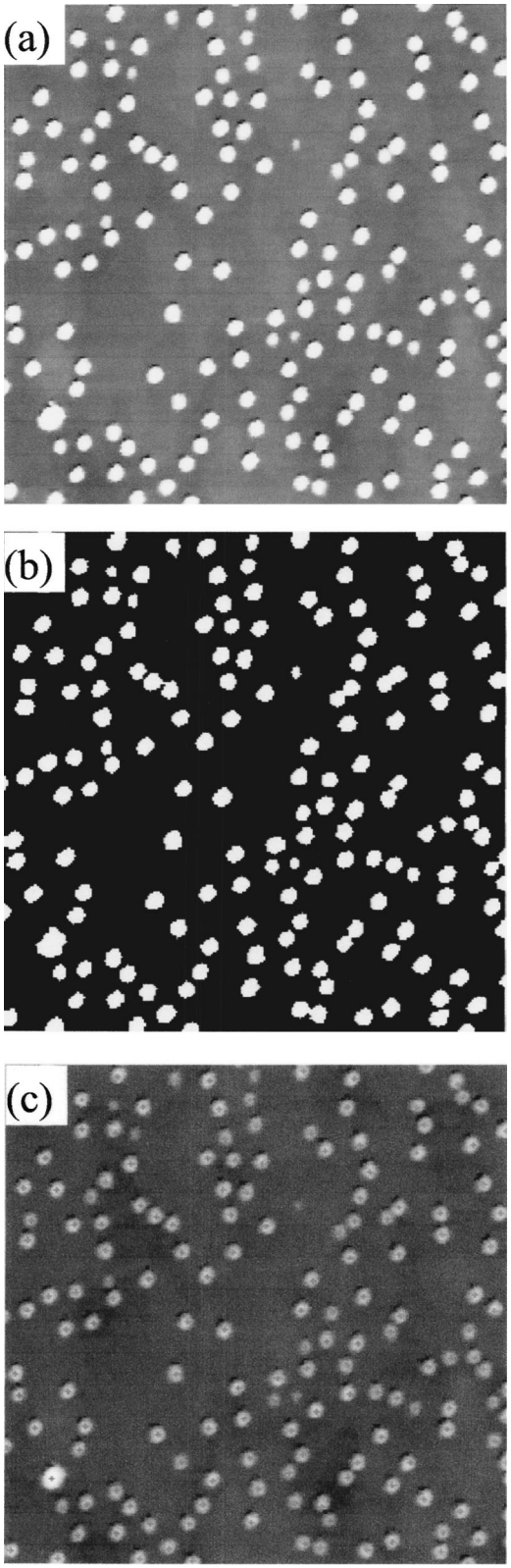

FIG. 4. (a) Original AFM image of InAs QDs (sample A), (b) image showing determined primitive area, and (c) the overlapped image of the position and morphology.

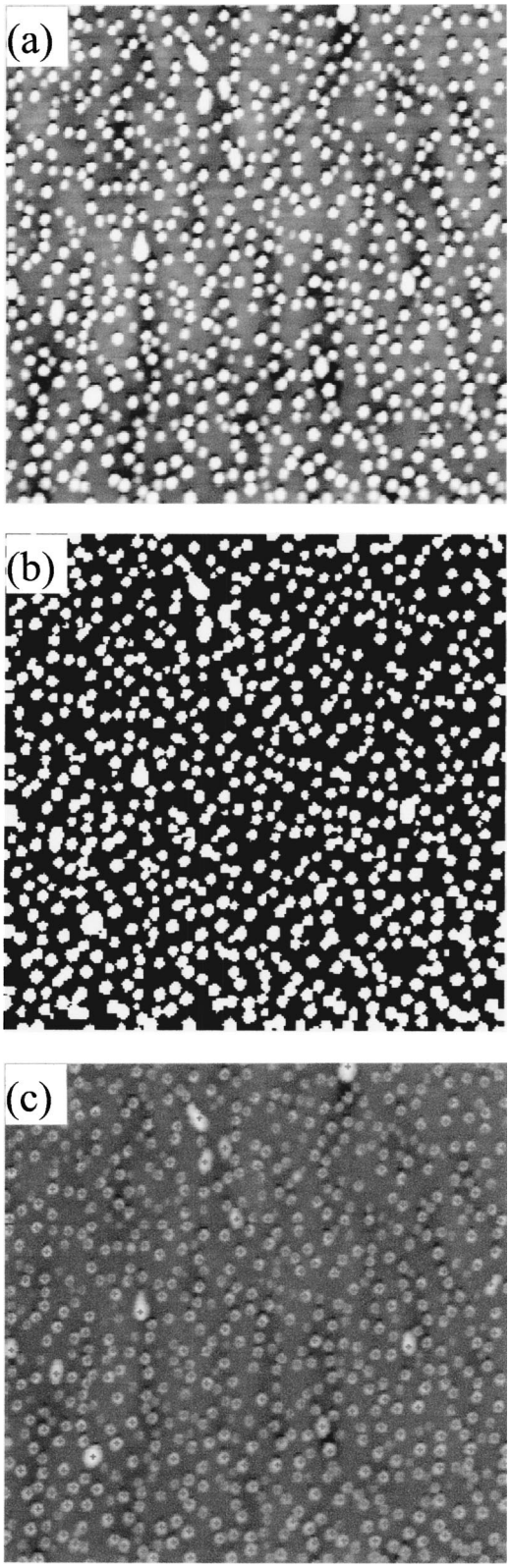

FIG. 5. (a) Original AFM image of small sized and densely formed InAs QDs (sample B), (b) image showing determined primitive area, and (c) the overlapped image of the position and morphology.

$$R_n(M_i) = R_{n+1}(M_i) \cup T_{M_i}[n], \tag{5}$$

where $R_n(M_i)$ may be regarded as a binary image. Suppose that the coordinates in $T[n]$ that are on the nth plane are marked white and all other coordinates are marked black. Then, when we look down on the xy plane at any decrement n of subsiding, we will see a binary image in which white points correspond to points in the image that are above the nth plane, that is $R_n(M_i)$. According to Eqs. (2) and (5), we can obtain final $R_{\mathrm{MIN}}(M_i)$ at stage $n = \mathrm{MIN}$. When the pro-

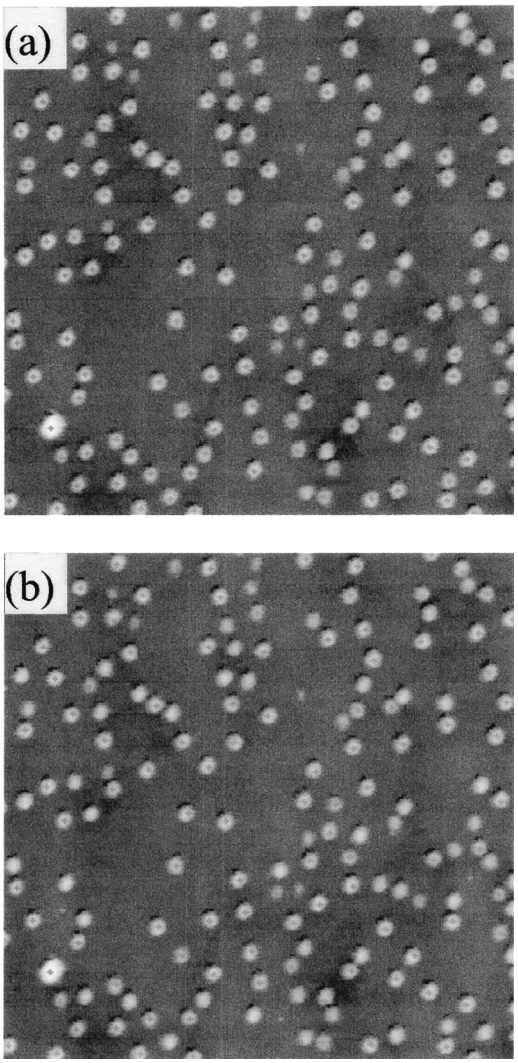

FIG. 6. QD detection result of sample A: (a) by threshold detection method and (b) by original watershed algorithm.

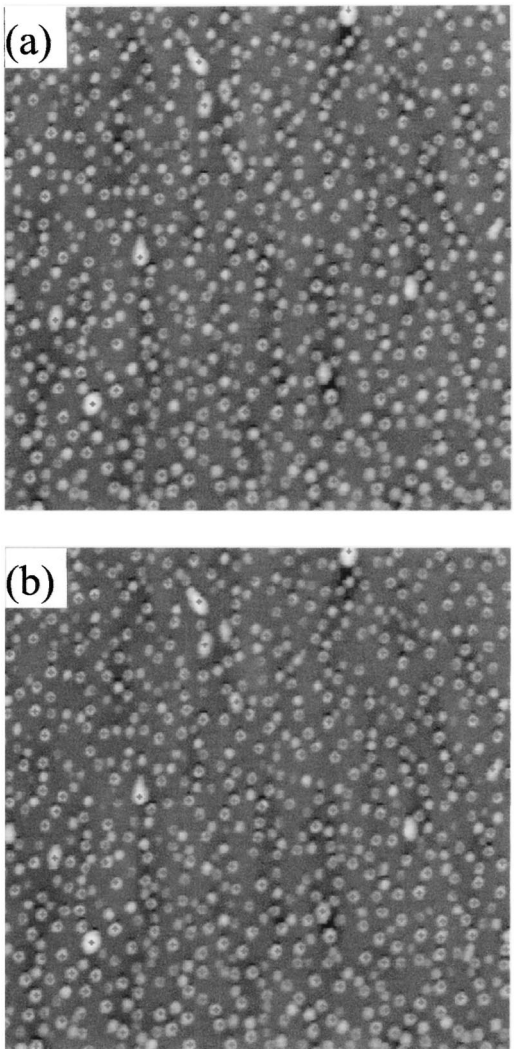

FIG. 7. QD detection result of sample B: (a) by threshold detection method and (b) by original watershed algorithm.

cessing is finished, C indicates the total number of regional maxima ($C = C\,\max$) and each $R_{\mathrm{MIN}}(M_i)$ indicates the final coordinates of the points in the region associated with regional maximum M_i. Therefore $R_{\mathrm{MIN}}(M_i)$ becomes a detected QD region. Finally, Fig. 3 shows a flowchart summarizing the algorithm.

As mentioned in the previous section, this algorithm produces the oversegmentation result. In particular, protrusions in flat region or noises are also detected as the QD's peak. Therefore, some characteristics of QD are used to determine whether the detected peak is a real QD or not. Below we list three characteristics of QD.

(i) The height of a peak should be sufficiently high from the base of QD—since the QD should have a meaningful volume, the height of QD should be reasonably high and the height of a protrusion of the flat should be small.

(ii) The diameter of a QD should be large enough—since the QD should have a reasonable volume, the diameter should also be reasonably large. This in turn, means that the gap between peaks should be large enough.

(iii) The QD has a round or polygonal shape. This means that a ratio between maximum radii on orthogonal coordinates should be reasonably acceptable.

Using these properties, each detected region is considered to be a QD region or not, and the regions that are determined not to be a QD are removed. The final data set $R_{\mathrm{MIN}}(M_i)$ is used to test the above three criteria. It corresponds to the marker explained in Sec. II B. Finally, the volume of the QD is calculated by adding small fractions lying inside between quantum dot boundaries at two consecutive height steps.

III. EXPERIMENTAL RESULTS AND DISCUSSION

We used AFM data obtained from a commercially available AFM.[8] The QD detection and volume determination algorithm was coded in C language and a common personal computer (PC) was used for the data processing. Since most of the modern AFMs use PCs for the probe control and image processing, our implementation can be directly applicable to them. Two different AFM images will be discussed. Prior to the QD detection, the original data went through the tilt correction and flattening process. All images have the same scale in the x and the y directions ($1\times1\ \mu\mathrm{m}^2$), and the

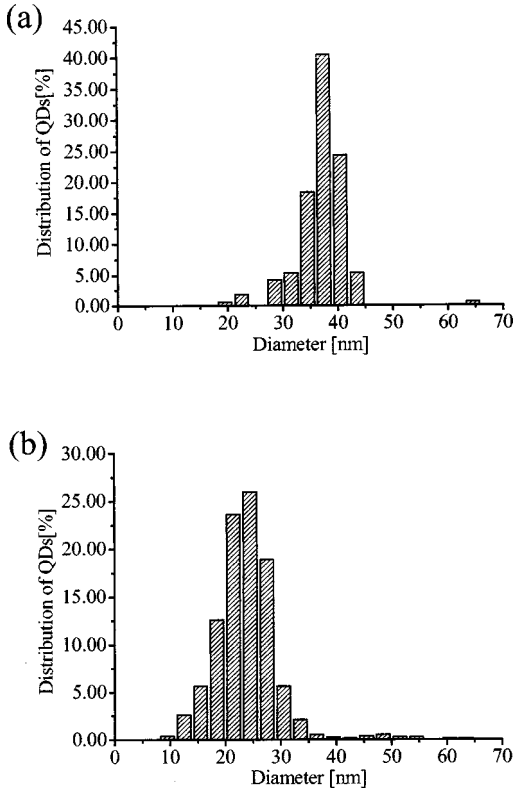

FIG. 8. Histogram of the distribution of the diameter in the elongated axis of the samples A and B.

scanning direction is *x*. The AFM image is comprised of 256×256 pixels with a lateral resolution of 3.906 25 nm. The scales in the *z* direction are set to display the whole range of the height data.

The QD sample used in this work has the following structure. Starting with semi-insulating (100) GaAs substrate, 300 nm of GaAs buffer layer and 3–3.6 monolayers (MLs) of InAs QDs are grown by the molecular beam expitaxy system. The growth temperature of the QDs is 480 °C. Further details about the QD growth are found in Refs. 12 and 13.

First, the image of Fig. 1(a) has gone through the developed detection/volume estimation algorithm. Figure 4(a) is the original image with 169 QDs easily discernible by the naked eye (sample A). QDs are randomly distributed throughout the entire surface. Figure 4(b) shows the QD's area determined after the processing of the image with the proposed algorithm. White regions reflect the detected QD area while black regions are the surface of the sample. According to the figure, the shape of the base of the QDs is rather circular. In this determination process, all of the 169 QDs are automatically detected, which agrees exactly with the manually counted result. In order to estimate the effectiveness of the proposed algorithm in determining the exact position of the QDs, we overlapped the determined QD area image with the peak position image in Fig. 4(c). As can be seen in this figure, the peak position is well inside of the QD, indicating the successful detection result.

Next image considered for QD detection is shown in Fig. 5(a) where approximately 752 QDs are determined by the naked eye (sample B). We did not include small QDs whose height variation was almost impossible to see. As shown in the figure, QDs are smaller than the previous image, and QDs are more densely formed which makes the detection more difficult. Manual QD counting and size determination of this amount become tedious and time-consuming work, therefore automation is mandatory. Figure 5(b) shows the obtained QD's area image, and Fig. 5(c) shows the area image overlapped with the peak position image. In this detection, 762 QDs have been automatically detected. About ten positions have been detected by oversegmentation, and this corresponds to 1.33% of the total detected QDs. Very low aspect ratio or small size of the QDs gives rise to the difference in the number of QDs determined by manual detection and the proposed detection method. More careful QD detection, taking into account the oversegmentation (discussed in Sec. II C), can reduce the detection error to less than 0.8%.

TABLE I. Diameter, height, and aspect ratio of sample A.

		Threshold	Original watershed	Proposed watershed
Average diameter in the elongated axis (nm)	Avg.	27.45	45.81	36.66
	σ	7.67	18.05	4.50
	Min	13.42	18.25	19.53
	Max	55.07	101.51	65.00
Height (nm)	Avg.	2.82	3.51	3.22
	σ	0.65	0.57	0.66
	Min	0.87	1.15	1.15
	Max	7.04	7.04	7.04
Aspect ratio	Avg.	0.102	0.076	0.088
	σ	0.085	0.032	0.015
	Min	0.065	0.063	0.058
	Max	0.128	0.07	0.108

A threshold detection and an original watershed algorithm have been applied to both samples A and B. A similar amount of optimization, as in the case of the proposed algorithm, has been done. Figures 6(a) and 6(b) show the results of QD detection for sample A, by the threshold detection and by the original watershed, respectively. The numbers of detected QDs are 153 (threshold) and 117 (original watershed). These values are much smaller than the manually detected number (169). Figures 7(a) and 7(b) show the results of QD detection for sample B, by the threshold detection and by the original watershed. In this case, the detected QDs are either 343 or 489, which are a lot fewer than the actual number (740). In both Figs. 6 and 7, we can also identify many detection spots which are artifacts.

Once the area and position of the QDs are determined, additional information such as the diameter *d*, height *h*, aspect ratio *A*, and volume *V* of the QDs can be automatically derived. The diameter of the QD is an important factor since it determines the quantum functionality of the device. Their statistical information such as size uniformity determined by the standard deviation of the QDs diameter is also useful in predicting the quality of the device to be fabricated.[21,22] For example, it is desired to obtain QDs with uniform size for optoelectronics application. Figures 8(a) and 8(b) show the distribution of the diameter of QDs in the elongated axis, of samples A and B, respectively. According to the histogram, the QDs of sample A are more uniform than those of sample

TABLE II. Diameter, height, and aspect ratio of sample B.

		Threshold	Original watershed	Proposed watershed
Average diameter in the elongated axis (nm)	Avg.	38.39	31.27	23.90
	σ	41.95	48.25	5.92
	Min	8.49	10.82	8.73
	Max	765.38	766.50	62.99
Height (nm)	Avg.	1.67	2.05	1.76
	σ	0.45	0.52	0.59
	Min	0.38	0.58	0.17
	Max	4.48	4.48	4.48
Aspect ratio	Avg.	0.043	0.066	0.073
	σ	0.011	0.011	0.017
	Min	0.045	0.054	0.019
	Max	0.006	0.006	0.12

B. This fact is reflected in the corresponding standard deviation values, which are 4.5 and 5.923 97 nm. Around 80% of the QDs of sample A are distributed in the diameter range of 33–43 nm and more than 95% are in the range of 32–45 nm. Other information about the geometry of samples A and B is summarized in Tables I and II, respectively. Additional information such as the minimum distance between QDs (not shown here) can be obtained, which would provide an analytical tool for the study of migration of QDs. For comparison, the geometry information obtained using the threshold detection and the original watershed are also shown. In the worst case, the diameter values are approximately 25% different from that of the proposed method. The standard deviation of the diameter is much larger than that of the realistic QD distribution when these conventional methods are used.

According to the previous investigations, the morphology of the QDs was revealed as lens shape, which can be approximated as conical for (100) substrates and pyramidal or prism like shape for (n11) substrates.[22–24] Therefore, we also calculated the volume assuming conical and pyramidal shape. As mentioned previously, the AFM data contain not only two dimensional information but also the height data, which provides very useful information for volume calculation. The volume estimation is considered to be an important procedure in the QD growth, since the amount of the source material consumed can be predicted precisely. The result of the volume determination can help the investigation of the quantitative adsorption and desorption process during the QD growth. The amount of the InAs deposited for QD growth was 3 and 3.6 MLs for samples A and B, respectively. During the QD growth, a wetting layer of 1.7 MLs is formed first (verified with reflection high-energy electron diffraction) and spontaneously InAs QDs are formed thereafter. Therefore, the amount of the InAs consumed for the formation of the QDs are 1.3 and 1.9 MLs for samples A and B, which correspond to a thickness of 0.394 and 0.576 nm, respectively. Corresponding volumes of InAs consumed for QDs regarding a square of 1×1 μm^2 are 394 000 and 576 000 nm^3 for samples A and B, respectively. Three types of volumes are calculated automatically. They are: as determined volumes calculated by adding up volume fractions at every step n, the volume assuming a conical QD with a radius and height derived from each $R_{\mathrm{MIN}}(M_i)$, and finally the volume assuming a pyramidal QD with a square base and height, where the base and height are derived again from each $R_{\mathrm{MIN}}(M_i)$. The formula of the volume used for conical and pyramidal shape can be expressed in terms of the diameter d and height h of the QD. We assumed that the base of the pyramid with a square base fit exactly inside a cone whose base is a circle with a radius $r=d/2$:

$$V_{\mathrm{con}}=(\pi/3)(d^2h/4), \tag{6}$$

$$V_{\mathrm{pyr}}=(1/3)(d^2h/2). \tag{7}$$

As a result the ratio between V_{con} and V_{pyr} becomes $\pi/2$.

All the volume calculation results are summarized in Tables III and IV. The results show differences between the theoretically calculated deposited InAs volumes and as determined QDs volumes. The volume of InAs QDs of sample A consumes in the growth was 394 000 nm^3 while the sum of the as determined QDs volume was 243 288 nm^3, corresponding to a ratio of 61.76%. A similar result is obtained for the sample B, where the ratio between consumed volumes and as determined volumes was 52.89%. The volume values obtained using the threshold detection and the original watershed are also shown in the tables. Both methods show

TABLE III. Estimated and automatically calculated volumes of sample A.

Model	Volume (nm^3)	Ratio (%)
Consumed	394 000	X
Conical model	203 310	51.6
Pyramidal model	128 709	32.7
Threshold method	103 708	26.32
Original watershed method	150 418	38.18
Proposed method	243 288	61.76

TABLE IV. Estimated and automatically calculated volumes of sample B.

Model	Volume (nm^3)	Ratio (%)
Consumed	576 000	X
Conical model	238 563	41.43
Pyramidal model	151 874	26.3
Threshold method	104 512	18.14
Original watershed method	194 075	33.69
Proposed method	304 478	52.89

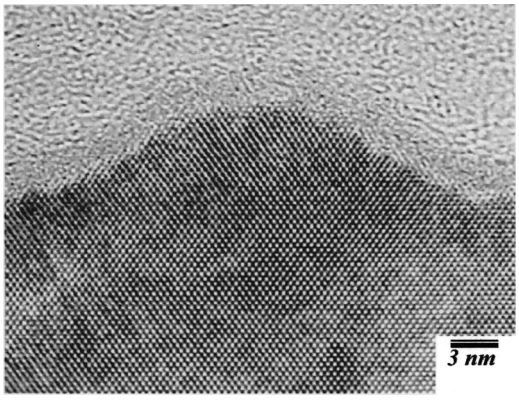

FIG. 9. TEM image of a typical QD in sample A.

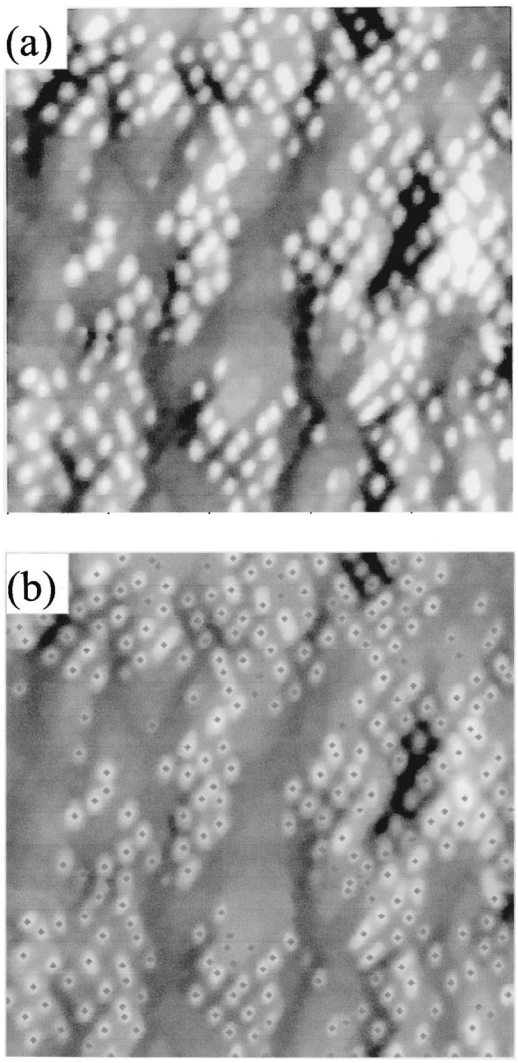

FIG. 10. Detection of QDs grown on a corrugated surface: (a) the original image and (b) the overlapped image of the position and morphology.

even smaller values than the proposed values. The main reason is that the conventional methods cannot detect a large portion of the existing QDs.

The fact that the volume calculated from the proposed method is smaller than the consumed volume can be attributed to the desorption process of the InAs, although a profound analysis and experiments are needed to figure out the exact mechanism of adsorption and desorption processes associated with the QD growth. Another uncertainty could be the convolution effect of the tip, which always causes some exaggeration in the measured QD diameter. In that case, real QD volume is always slightly less than the as determined volumes given above. Figure 9 shows the transmission electron micrograph image of a typical QD in sample A. Clear image of the crystal lattices enables accurate estimation of the QD diameter and height. The accurate diameter and the height obtained from this TEM image are 30 and 4.8 nm, respectively. While the accurate diameter is in reasonable agreement with the average diameter obtained from the proposed method, the height of the proposed method is underestimated. The radius of curvature of the used tip is 10 nm, and such uncertainty in height value is consistent with the curvature of the tip. Another important point is that the average diameters obtained from the threshold and the original watershed show much larger discrepancies than the proposed method.

Finally, we applied the proposed algorithm to the detection of QDs grown on a corrugated surface,[13] where the height of the base of the QDs differs by more than 6 nm, in some cases. By using only thresholding method the detection of the QDs grown on valley area will be impossible. Figure 10(a) shows the original AFM image of the QDs grown on such a corrugated surface. The total number of QDs identified by the naked eye is 282. After the detection procedure the number was 280 as shown in Fig. 10(b). But in the detection procedure eight QDs were not detected, while ten QDs are detected wrongly, giving a detection error of 6.4%. Perhaps, this is the limit of the automation, or we need more advanced approaches such as the two-dimensional partitioning of the image by selecting areas of similar height and applying the proposed algorithm separately. Finally, we should emphasize that the QD detection and volume estimation are totally automated and any type of manual handling is not involved.

ACKNOWLEDGMENTS

The authors would like to thank Dr. Kwang Moo Kim and Dr. Jin Dong Song of the Korea Institute of Science and Technology for providing InAs QD samples. The work at Korea University was supported by the Brain Korea 21 Project in 2003.

[1] R. Wiesendanger, *Scanning Probe Microscopy and Spectroscopy* (Cambridge University Press, Cambridge, 1994).
[2] P. K. Hansma *et al.*, Appl. Phys. Lett. **66**, 1738 (1994).
[3] *XE-100 High Accuracy SPM*, User's Manual, PSIA, Seoul, Korea.
[4] V. Yu. Yurov and A. N. Klimov, Rev. Sci. Instrum. **65**, 1551 (1994).
[5] R. C. Barrett and C. F. Quate, Rev. Sci. Instrum. **62**, 1393 (1991).
[6] G. Antonio, G. Cidade, G. Weissmuller, and P. M. Bisch, Rev. Sci. Instrum. **69**, 3593 (1998).
[7] P. Markiewicz and M. C. Goh, Rev. Sci. Instrum. **66**, 3186 (1995).
[8] C. Hyon, S. Oh, H. Kim, S. Sull, S. Hwang, D. Ahn, Y. Park, and E. Kim, Rev. Sci. Instrum. **73**, 3245 (2002).
[9] S. K. Jung, C. K. Hyon, J. H. Park, S. W. Hwang, D. Ahn, M. H. Son, B. D. Min, Y. Kim, and E. K. Kim, Appl. Phys. Lett. **75**, 1167 (1999).
[10] H. Muramatsù, N. Chiba, K. Homma, K. Nakajima, T. Ataka, S. Ohta, A. Kusumi, and M. Fujihira, Appl. Phys. Lett. **66**, 3245 (1995).
[11] M. Badaye, W. Ting, K. Fukushima, N. Koshizuka, T. Morishita, and S. Tanaka, Appl. Phys. Lett. **67**, 2155 (1995).
[12] C. K. Hahn, Y. J. Park, E. K. Kim, S.-K. Min, S. K. Jung, and J. H. Park, Appl. Phys. Lett. **73**, 2479 (1998).
[13] K. M. Kim, Y. J. Park, Y. M. Park, C. K. Hyon, E. K. Kim, and J. H. Park, J. Appl. Phys. **92**, 5453 (2002).
[14] G. S. Pingali and R. Jain, Proceedings of the Instrumentation and Measurement Technology Conference, Irvine, CA, May 1993, p. 327.
[15] R. C. Gonzalez and R. E. Woods, *Digital Image Processing*, 2nd ed. (Prentice-Hall, Englewood Cliffs, N.J., 2001).
[16] J. M. Gauch, IEEE Trans. Image Process. **8**, 69 (1999).
[17] K. Haris, S. N. Efstratiadis, N. Maglaveras, and A. K. Katsaggelos, IEEE Trans. Image Process. **2**, 1684 (1998).
[18] A. Tremeau and P. Colantoni, IEEE Trans. Image Process. **9**, 735 (2000).
[19] F. Meyer and S. Beucher, J. Visual Commun. Image Represent **1**, 21 (1990).
[20] P. Salembier and M. Pardas, IEEE Trans. Image Process. **3**, 639 (1994).
[21] D. Bimberg, M. Grundmann, and N. N. Ledentsov, *Quantum Dot Heterostructures* (Wiley, Chichester, 1999).
[22] D. Leonard, K. Pond, and P. M. Petroff, Phys. Rev. B **50**, 11687 (1994).
[23] K. Yamaguchi, T. Kaizu, K. Yujobo, and Y. Saito, J. Cryst. Growth **237–239**, 1301 (2002).
[24] J.-S. Lee, K. Nishi, and Y. Masumoto, J. Cryst. Growth **221**, 586 (2000).